Flow Induced Fluctuations Create a Granular Fluid: Effective Viscosity and Fluctuations

Nichol, K.M.; Hecke, M.L. van

Flow-induced agitations create a granular fluid: Effective viscosity and fluctuations

Kiri Nichol and Martin van Hecke
Kamerlingh Onnes Lab, Universiteit Leiden, Postbus 9504, 2300 RA Leiden, The Netherlands
(Received 30 October 2011; published 28 June 2012)

We fluidize a granular medium with localized stirring in a split-bottom shear cell. We probe the mechanical response of quiescent regions far from the main flow by observing the vertical motion of cylindrical probes rising, sinking, and floating in the grains. First, we find that the probe motion suggests that the granular material behaves in a liquid-like manner: high-density probes sink and low-density probes float at the depth given by Archimedes' law. Second, we observe that the drag force on moving probes scales linearly with their velocity, which allows us to define an effective viscosity for the system. This effective viscosity is inversely proportional to the rotation rate of the disk which drives the split bottom flow. Moreover, the apparent viscosity depends on radius and mass of the probe: despite the linear dependence of the drag forces on sinking speed of the probe, the granular medium is not simply Newtonian, but exhibits a more complex rheology. The decrease of viscosity with filling height of the cell, combined with the poor correlation between local strain rate and viscosity, suggests that the fluid-like character of the material is set by agitations generated in the stirred region: the relation between applied stress and observed strain rate in one location depends on the strain rate in another location. We probe the nature of the granular fluctuations that we believe mediates these nonlocal interactions by characterizing the small and random up and down motion that the probe experiences. These Gaussian fluctuations exhibit a mix of diffusive and subdiffusive behavior at short times and saturate at a value of roughly 1/10th of a grain diameter longer times, consistent with the picture of a random walker in a potential well. The product of crossover time and effective viscosity is constant, evidencing a direct link between fluctuations and viscosity.

DOI: 10.1103/PhysRevE.85.061309 PACS number(s): 47.57.Gc, 83.80.Fg

I. INTRODUCTION

What governs the flow of granular media? At the grain level, interactions are mediated by collisions and contacts [1]. While rapid flows where collisions dominate can be described by advanced kinetic theories [2], and the understanding of flows where both contacts and collisions are important has recently advanced tremendously [3,4], it remains difficult to describe slow flows where enduring contacts dominate the interactions.

Aspects of such slow grain flows can be captured by a frictional rheology in which the friction laws acting at the grain scale are translated to effective friction laws for the stresses acting at a coarse-grained level [5–7]. In such a Mohr-Coulomb picture, granular media remain jammed when the ratio of shear τ to normal stresses P is below a critical value given by an effective friction coefficient μ, while slowly flowing grains exhibit stresses close to the yielding criterion: $\tau/P \gtrsim \mu$.

This framework is, however, not complete. The combination of rate independence and a sharp yielding criterium leads to a description which predicts the localization of flows in shear bands of vanishing width and a corresponding sharp separation between stationary zones and flowing zones [5]. However, in experiments shear bands are found to be of finite width and the boundary between flowing and stationary zones is not sharp, with creep flow occurring even far away from the main shear band [8–13]. The first key question is therefore: What is the nature of the nearly stationary zones far away from the main flow? A second key question is motivated by the observation that, for slow flows, the flow rate is independent of the stresses. But if the flow rate is not determined by the stresses, what then is the physical mechanism that sets the flow rate of slow granular flows [3,5,7]?

In the experiments described here, we address these questions by locally stirring glass beads in a split-bottom shear cell while probing the mechanical response of the essentially quiescent regions near the surface, away from the shear band. Details of the setup can be found in Sec. II A.

In the absence of stirring, the grains exhibit the usual physical properties of a static sand pile, and the beads will support an object of moderate mass placed on the surface, an observation which indicates that, collectively, the beads exhibit a yield stress. However, once the disk in the bottom of the container starts rotating, an intruding object will immediately begin to sink into the beads. An object which is denser than the mixture of beads and air in the container will continue to sink until it is completely submerged. Meanwhile, a low-density object placed in the beads while the disk is rotating will rise or sink until it floats at a certain equilibrium depth.

These behaviors are surprisingly liquid-like, which motivates us to treat the granular medium as a fluid and posit questions about the macroscopic properties of the system. Does the granular medium exhibit a yield stress? What parameters set the sinking speed of the probe? What physical mechanism causes the probes to sink and float?

First, we will establish that the equilibrium depth of a low-density object rising in the grains is equal to the equilibrium depth of that same object sinking in the grains. This demonstrates that our granular liquid does not exhibit a yield stress: if there were a finite flow threshold, sinking probes would get stuck at a different depth than rising probes. Moreover, we find that the equilibrium depth of the probe can be predicted from the effective density of the granular medium and the dimensions of the probe: objects floating in the grains obey Archimedes' rule.

Second, we have found that the trajectory of floating probes as they sink to their equilibrium depths is exponential in time. Since the sum of the gravitational and buoyant forces is linear

in the deviation from the equilibrium position, the exponential relaxation strongly suggests that the drag forces on a moving probe are linear in velocity, just as for viscous drag. From the gravitational force, buoyant force, and vertical motion of a sinking (or rising) object, we thus define and extract an effective viscosity. This viscosity is inversely proportional to the disk rotation rate. Unlike a Newtonian liquid, the viscosity also depends on radius (R) and mass (M) of the probe: although we are limited to studying probes with a small range of radii and mass, our observations suggest that the viscosity scales inversely with $(M/R^2)^2$. We also observe that the viscosity increases when the shear cell is filled to larger heights and depends weakly on the vertical position of the probe.

Third, we enquire if the local flow rate under the probe sets the effective viscosity. Even though the residual flow in the grains is small, it is not zero. Does this local, residual flow set the effective viscosity, or is the effective viscosity determined by agitations driven by flow further away? Using a rheometer, we have measured the local flow rate along the central axis of the rotating disk for several different filling heights and compare this rate to the local viscosity as determined from sinking probe experiments. We find that the local strain rate and viscosity are very poorly correlated: the flow rate can decrease over a factor of 1000 while the viscosity changes by less than a factor of three.

We believe that fluctuations in the granular medium mediate the interactions between a flowing zone in one location, and the effective viscosity experienced in another location. We have probed these fluctuations by characterizing the random fluctuations in the probe position. We find that these fluctuations are Gaussian, and that their root mean square exhibits a mix of diffusive and subdiffusive behavior at short times and saturates at a value of roughly 1/10th of a grain diameter for times longer than a crossover time, consistent with the picture of a random walker in a potential well. The product of crossover time and effective viscosity is constant.

We conclude that the relation between applied stress and observed strain rate in one location depends on the strain rate in another location [14,15]. Moreover, despite the linear relationship between the drag force and the sinking speed of the probe, the granular medium is not simply Newtonian. Finally, our data strongly suggest a direct link between fluctuations and (effective) viscosity of the granular medium. All these are crucial ingredients for the development of better models of slow granular flows [15–17].

II. AGITATION OF GRAINS THROUGH FLOW

We induce shear flow in a container of glass beads by rotating a disk in the bottom of the vessel, a split bottom setup. The fluid-like characteristics of the beads can then be probed by observing the motion of a low-density object sinking (or rising) in the grains. Here we discuss our setup and experimental procedure and main phenomenology.

A. Experimental setup and procedure

In this experiment, a split bottom cell (Fig. 1) is filled with 1 mm glass beads to a depth H ranging from 45 to 80 mm. The sidewalls are roughened by teeth of length 2 mm

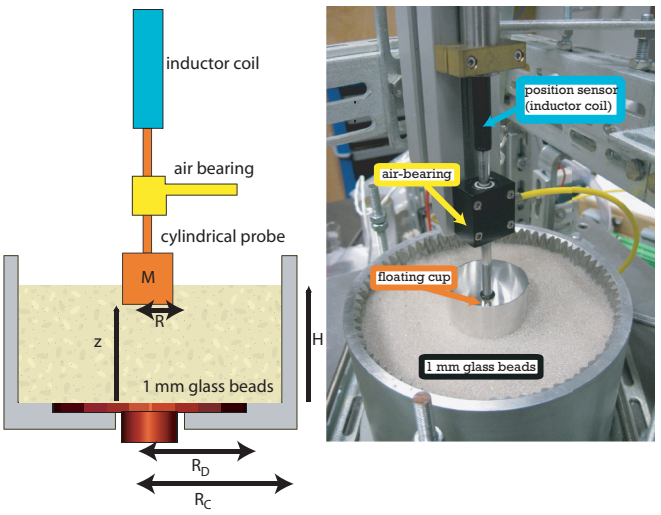

FIG. 1. (Color online) The spinning disk (radius $R_D = 60$ mm) revolves in the bottom of a cylindrical container (radius $R_C = 80$ mm) which has been filled to a height H with 1 mm glass beads. The distance between the spinning disk and the bottom of the probe is denoted by z. The hollow cylindrical probe has mass M and radius R. A photo of the experimental setup is on the right.

and height 2.5 mm, which are machined into the walls of the container. Because of these teeth the radius of the container varies between $R_C = 80$ and 82.5 mm.[1] The bottom disk has a radius of $R_D = 60$ mm and is roughened by hemispherical dimples with a diameter of 3 mm. The disk is driven at a rate Ω, either with a stepper motor attached to a belt or directly by a stepper motor; the precise driving mechanism has only a negligible effect on the behavior of the system, and we conclude that there are no spurious vibrations introduced when the motor drives the disk directly. The humidity of the system is controlled by placing the apparatus in a small plastic tent and allowing dry air escaping from the air bearing (Fig. 1) to flow over the grains. The humidity is maintained at 7%–9% at room temperature. This setup produces granular shear flows which have already been described in detail [11,12,18–22].

In order to investigate the rheological properties of the system we observe the motion of a probe moving vertically in the grains. The probe consists of a hollow closed cylinder attached to a shaft which passes through an air bearing and into a DC Fastar FS1K LVDT sensor (Fig. 1). The air bearing fixes the horizontal position of the probe while allowing the cylinder to rotate and to move freely in the grains in the vertical direction. Cylinders immersed in the beads have radii ranging from 7 to 30 mm, and the mass of the probe (m) can be varied by adding additional weights to the cylinder. The position of the probe is measured by the LVDT sensor, which has a resolution of 0.002 mm and a range of 51 mm with a linearity of $\pm 0.15\%$. Electronic noise in the signal is reduced by sampling at a rate of 250 Hz and then averaging over 10 points.

The filling height H (Fig. 1) is not measured directly because the volume changes as the grains compact and dilate;

[1]Both the main flow and our immersion experiments are far away from the sidewalls; R_C is sufficiently large so that its precise value does not influence the flow.

packing fraction is not a constant in a granular medium. Instead, we control the total mass of the grains in the container, even though we report the filling height H. A filling height of $H = 60$ mm measured prior to shearing the system corresponds to 2.4 kg of grains, and each 5 mm increment in the filling height requires the addition of 200 g of grains.

Given that the average radius of the shear cell is 81.5 mm we estimate a packing density $\rho \approx 1.92$ g/cm^3. Since grains pack less densely near sidewalls [23], we can also obtain the density of the medium by measuring the volume of the grains placed in beakers of increasing radius and extrapolating to infinite radius. This yields an independent estimate the density of well-compacted grains to be 1.92 ± 0.05 g/cm^3. Of course, when the beads are sheared they dilate, and the filling height of the sheared beads, $H(0)$, is typically 1 to 2 mm larger than the static filling height. When this dilation is taken into account, the typical densities encountered in our experiment are 1.86 ± 0.1 g/cm^3.

Protocol—In order to minimize memory effects the grains are stirred with a rod prior to beginning a measurement. The surface of the granular medium is leveled by smoothing it with a flat plate while spinning the disk at a rate of 0.5 rps for 20 s. Exploring other initial procedures yields no evidence that the initialization process influences the long-time dynamics of the probe: the random run-to-run variation in the probe motion is larger than variation observed for different preparation methods.

At the start of a sinking probe experiment, the probe is held at a position just above the surface of the grains (1–2 mm) and then released when the disk at the bottom of the container begins spinning. Prior to beginning an experiment with a rising probe the probe is submerged in the beads; details of the submersion procedure do not systematically influence the long-time dynamics of the probe.

B. Phenomenology

In our experiment, shear flow is generated in a container of glass beads by rotating a disk in the bottom of the vessel (Fig. 1). In the absence of shear, objects placed on the surface of the granular medium will become stuck after sinking a short distance (only a few mm for probes with a large mass and small area). In other words, the undriven granular system exhibits a yield stress.

However, the behavior of the grains changes dramatically when the beads are sheared by the rotating disk: a heavy object placed at the surface will immediately begin sinking and will continue sinking until it is submerged. Figure 2(a) shows a dramatic example, where a heavy steel ball sinks in the grains over a time scale of tens of seconds. Meanwhile, low-density objects either sink or rise until they are floating in the grains (Fig. 2). In the remainder of this paper, we will examine how the vertical motion of the probe $z(t)$ depends on the rotation speed of the disk (Ω), filling height of grains in the container (H), probe mass (M), and radius (R).

Note that for most of our experimental conditions, the amount of surface flow that we detect in absence of a probe is very small: at $H = 60$ mm, the residual flow at the surface is more than three orders of magnitude slower than the disk rotation rate [12,21]. For the sample probe trajectory shown in Fig. 2(a) the residual flow at the surface is approximately one rotation per 3 h. We will discuss the role of local flow rate in more detail in Sec. IV C.

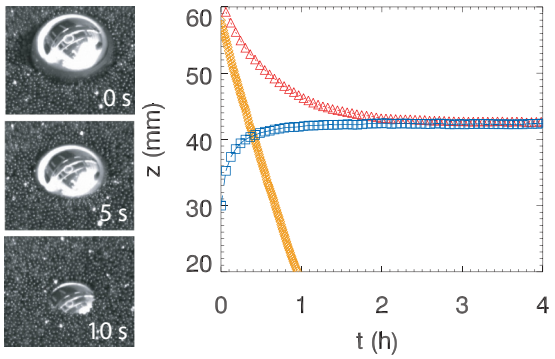

FIG. 2. (Color online) Examples of probe motion for filling height $H = 60$ mm and disk rotation speed $\Omega = 0.1$ rps. Left: Snapshots of a steel ball (diameter 25 mm, mass 64 g), as it sinks in the grains. When the disk is not rotating, the ball remains resting at the surface, as shown in the top panel. Right: Trajectories of probes moving in the fluidized grains. The orange line going straight down indicates the sinking of a high-density probe ($M = 48$ g, $R = 9$ mm). A second, low-density probe ($M = 40$ g, $R = 20$ mm) floats in the grains. This probe sinks if initially placed above the equilibrium depth (red triangles) and rises if placed below the equilibrium depth (blue squares).

III. ARCHIMEDES' LAW IN A GRANULAR FLUID

As shown in Fig. 2(b), low-density probes sink or rise to a well-defined equilibrium depth z_{eq}. The probe position as a function of time for several rising and sinking experiments at $H = 60$ and 50 mm is plotted in Figs. 3(a) and 3(c). These trajectories illustrate that probes of a given mass reach the same equilibrium depth in sinking and rising experiments for a wide range of parameters, and that when the mass of the probe is increased, the probe descends to a lower equilibrium position.

Examining a brief segment of the probe trajectory reveals that $z(t)$ exhibits tiny, Gaussian fluctuations around the mean position z_{eq} [Fig. 3(b)]. Variations in the value of z_{eq} achieved in different experimental runs are small and of the order of 0.2 mm, one-fifth of grain diameter.

That the equilibrium position does not depend on whether the probe is initially below or above z_{eq} suggests that our granular system does not exhibit a yield stress; if there were a finite flow threshold, sinking probes would get stuck at a shallower depth than rising probes. This observation, together with the the observation that heavier probes have a deeper equilibrium depth [Fig. 3(c)], motivates describing the probe behavior using Archimedes' law, in which the equilibrium depth is predicted by the balancing the buoyant force and the gravitational force.

Let us now propose that a cylindrical probe floats at an equilibrium depth, $z = z_{eq}$. For an infinite container, and in the absence of any granular and dilatancy effects, Archimedes' law reads

$$-Mg + \pi R^2 \rho g[H(0) - z_{eq}] = 0, \qquad (1)$$

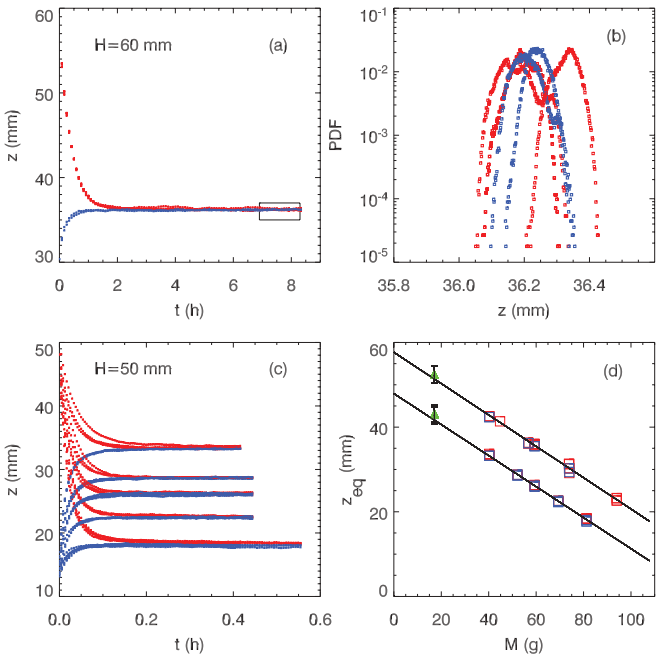

FIG. 3. (Color online) Floating probes behave according to Archimedes' law. All experiments are conducted with a probe of radius $R = 20$ mm and at a disk rotation speed of $\Omega = 0.1$ rps. (a) Examples of probes of sinking and rising to their equilibrium depth. Here $H = 60$ mm and the probe mass is 57 g. (b) Probability densities of the probe position near equilibrium (the last 15% of each data set) for three observations of a sinking probe (red, light gray) and three observations of the same probe as it rises in the grains (blue, dark gray); no systematic deviation between the probe positions of rising and sinking probes can be observed ($M = 57$ g, $z_{\rm eq} \approx 36$ mm). (c) Sinking and rising probes for $H = 50$ mm; note the difference in time scale in comparison to panel (a). (d) The equilibrium depth as a function of probe mass for $H = 60$ (upper data set, intercept 56.89 mm, slope -0.358 mm/g) and $H = 50$ (lower data set, intercept 47.93 mm, slope -0.366 mm/g). The green data points at $M \approx 20$ g (triangles) are obtained by imaging the position of a very light probe with a camera.

where ρ denotes the effective density of the granular medium, and $H(0)$ is the filling height of the container prior to the introduction of the probe [note that the medium dilates during shear, so that $H(0)$ is typically 1 mm larger than the initial filling height H]. The change in the filling height due to dilation of the beads can be estimated by dropping a probe on to the surface of the granular system and measuring the height at which the probe is no longer falling.

There are several corrections that we need to take into account. First, since the container has a finite radius R, immersion of a probe will displace grains and raise the "fluid" level. We have therefore calculated the height of the beads in the container, $H(z)$, as a function of the depth reached by the probe z. We assume that the beads are not dilated or compacted when the probe is immersed so that the total volume of the beads is conserved:

$$R_C^2[H(z) - H(0)] = R^2[H(z) - z]. \tag{2}$$

Solving for $H(z)$ in terms of $H(0)$ and z and replacing $H(0)$ in Eq. (1) with $H(z)$ yields

$$-Mg + \pi R^2 \rho g \frac{R_C^2}{R_C^2 - R^2}[H(0) - z_{\rm eq}] = 0. \tag{3}$$

There are two additional corrections to the equilibrium depth, which stem from the fact that grains pack less efficiently close to boundaries. This observation suggests that the effective radius of the probe $\tilde{R}$ may be somewhat larger than the real value: $R < \tilde{R} < R + R_{\rm grain}$. Similarly, grains pack less densely against the bottom of the probe than in the bulk, so the measured equilibrium depth is $\delta H \approx$ one grain diameter higher than expected.

When these finite size corrections into account, the equilibrium position, $z_{\rm eq}$ is given by

$$z_{\rm eq} = H_0 - \delta H - \frac{M}{\pi R^2 \kappa \rho}. \tag{4}$$

Here all finite size corrections are combined in the effective parameters δH and $\tilde{R}$, while $\kappa = 1 + (\tilde{R}/R_C)^2$ describes the change in $H(z)$ as the probe sinks and displaces beads. The value of δH is approximately 1 mm, while for a probe of $R = 20$ mm, $1 + (R/R_C)^2 \approx 1.06$, and $1 < (\tilde{R}/R)^2 < 1.05$. The value of κ should therefore lie between 1.06 and 1.11.

The measured equilibrium position is calculated by fitting the observed probe position as a function of time to a sum of exponentials, as described in Sec. VI. In Fig. 3(d) we plot the equilibrium depths of rising and sinking probes as function of probe mass for both $H = 50$ and 60 mm. The green data points are obtained for very light probes, which, to reduce the mass of the probe are not attached to an inductor rod. The equilibrium position of the probe is therefore obtained (with less accuracy) by taking photos at intervals as the probe sinks into the grains.

As illustrated in Fig. 3(d), the equilibrium depths can be described by Eq. (4). The slope of both fits is given by $(\pi R^2 \kappa \rho)^{-1}$ and is consistent with the density of the grains and our previous estimate of κ. The fit for the $H = 60$ mm data yields $\kappa\rho = 2.05 \pm 0.05$ g/cm^3, while the fit for $H = 50$ mm data yields $\kappa\rho = 2.04 \pm 0.02$ g/cm^3. From our estimate of the density (1.86 ± 0.1 g/cm^3), it follows that $\kappa \approx 1.1 \pm 0.05$, which lies within the expected range. The finite size correction δH is on the order of a grain diameter: $\delta H = 2.1$ mm for $H = 50$ mm and $\delta H = 3.1$ mm for $H = 60$ mm.

We conclude that Archimedes' law describes the equilibrium depths of our probes accurately, provided that the dimensions of the container and finite size effects are properly taken into account. Note that Archimedes' law has also been observed in a granular system in which the lateral boundaries are vibrated [24], but this driving appears far more vigorous than in our system. Also note that similarity between the equilibrium depth for sinking and rising probes, as well as their good agreement with Archimedes' law, implies that segregation effects are not important in our experiment; this is consistent with the fact that our experiments take place far from the flowing zone.

IV. VISCOUS DRAG IN A GRANULAR FLUID

Now that we have established the underlying mechanisms and the forces acting on stationary probes, we turn our attention to the probe dynamics: the motion of probes when they are sinking or rising. We will first establish that the approach of probes toward their equilibrium depth is exponential, which allows us to define an effective viscosity η. We will then measure how η varies with filling height H, disk rotation speed, Ω, probe depth z, mass M, and radius r. Moreover, we will explore the effect of placing the probe off center. Our main conclusion is that, although the drag forces on moving probes scale approximately linearly with probe velocity, the drag forces depend strongly on the pressure exerted by the probe and the filling height; there is not a simple, single effective viscosity in our fluid.

A. Equation of motion

As Fig. 3(c) suggests, a probe approaches its equilibrium depth exponentially in time. To make this more precise, we plot the log of z–$z_{\rm eq}$ versus time (Fig. 4). The linear nature of this relationship demonstrates the exponential character of the probe motion for both sinking and rising probes. Because the sum of the gravitational force and the buoyant force on the probe is proportional to z–$z_{\rm eq}$, the exponential approach to equilibrium implies that the probe experiences a drag force proportional to its velocity: viscous drag.

The observations of both Archimedes' law and of exponential trajectories of probes as they approach equilibrium suggests that three forces act on the probe: gravity (Mg), buoyancy $[\pi R^2 \rho g \frac{R^2}{R^2-r^2}(H - z_{\rm eq})]$, and a dissipative force analagous to viscous drag, $2\eta R \frac{dz}{dt}$. Although Eq. (4) takes the corrections to the effective radius and variation of the packing density near the probe into account, these corrections are small, and we will exclude them from our subsequent analysis.

If we assume that inertial effects can be ignored so that the motion of the probe is overdamped, it is possible to extend Eq. (3) to describe the motion of the probe away from equilibrium:

$$-Mg + \pi R^2 \rho g \frac{R_C^2}{R_C^2 - R^2}[H(0) - z(t)] - 2\eta R \frac{dz}{dt} = 0. \quad (5)$$

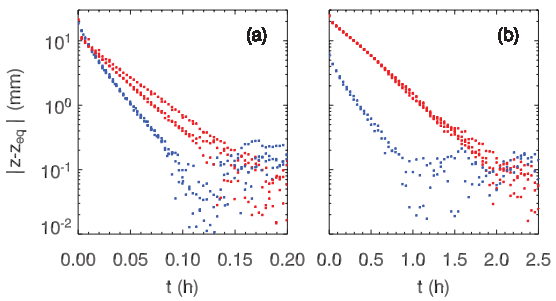

FIG. 4. (Color online) Log of $z - z_{\rm eq}$ as a function of time. The approximately linear behavior is suggestive of viscous drag. (a) $H = 60$ mm. (b) $H = 50$ mm. The two red (light gray) curves denotes experiments in which the probe sinks and in both panels lie above the two blue (dark gray) curves, which are taken from experiments for which the probe rises.

1. Determining viscosities

Using the position of the probe as a function of time $[z(t)]$ we can determine the viscosity as a function of the parameters M, R, Ω, H, and z [Eq. (6)]. In particular this allows us to determine whether the viscosity varies with the probe depth z; there is no *a priori* reason for the effective viscosity to be constant throughout the entire system. Although we previously observed that $z(t)$–$z_{\rm eq}$ is exponential (Fig. 4), it is important to stress that the main implication of the *approximately* exponential form of this relaxation is that it rules out, for example, a power law relationship between the drag force and probe motion; in leading order, the drag force is linear in the probe speed. In fact, we do observe spatial gradients in η, although the variations are rarely larger than a factor of two over the entire trajectory of the probe and are much smaller than the variations in local strain rate (see Sec. IV C).

To calculate the probe velocity, dz/dt, we numerically differentiate $z(t)$ over a time interval δ:

$$v(t) = [x(t + \delta/2] - x[t - \delta/2)]/\delta. \quad (6)$$

Time scales for the motion of the probes vary by several orders of magnitude when M, R, H, or Ω is changed. The total duration of each run is long enough to observe the probe until it is nearly submerged or until it is well equilibrated. The time interval δ is also adjusted to minimize noise: δ is proportional to the total duration of the data set.

The filling height of the sheared beads prior to the introduction of a probe $[H(0)]$ is typically 1 to 2 mm larger than the static filling height. As described previously (Sec. II A) this dilation can be measured by observing the position at which a light falling probe slows dramatically, the point at which the probe contacts the grains. For heavy probes the point at which the probe contacts the grains is harder to discern, so $H(0)$ is simply set to the static filling height H plus 1 mm.

Extracting reliable values of the viscosity close to the equilibrium depth of floating probes is complicated by two factors. First, fluctuations dominate the motion of the probe in this region: close to $z_{\rm eq}$, both $v(t)$ and $z(t)$–$z_{\rm eq}$ go to 0, and so the error in the viscosity, which is proportional to $[z(t) - z_{\rm eq}]/v(t)$, diverges. We therefore ignore the calculated viscosities within 1 mm of the equilibrium depth. Second, extracting reliable values of the viscosity close to equilibrium is possible only if the bead density and filling height are such that the buoyant force and gravitational force are equal and opposite at equilibrium. To minimize this problem, we use the fitted value for $z_{\rm eq}$ [Eq. (8)] to calculate a best estimate for the density. For probes too heavy to float in the grains this problem does not arise, and the measured density of 1.92 ± 0.05 g/cm^3 is used.

2. Sinking vs rising

Close inspection of Fig. 3(c) suggests that the probe appears to rise more quickly than it sinks at $H = 60$ mm. This is also apparent in the plots of $\ln[z(t)$–$z_{\rm eq}]$ in Fig. 4(a). Note that near the equilibrium depth, $\ln[z(t)$–$z_{\rm eq}]$ is very sensitive to the value of $z_{\rm eq}$. Surprisingly, the difference between sinking and rising probes appears to be less pronounced for $H = 50$ mm [Fig. 4(b)].

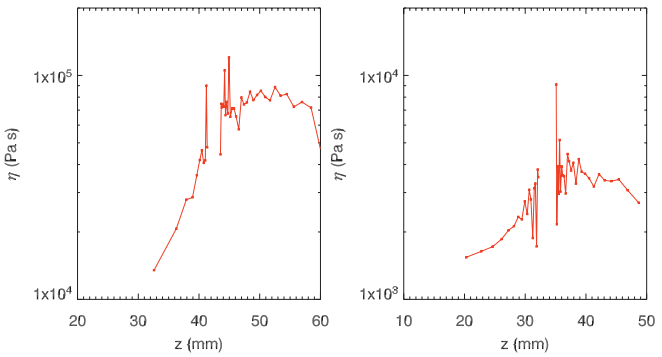

FIG. 5. (Color online) Viscosity as a function of probe position for filling height $H = 60$ mm (left) and $H = 50$ mm (right) for $\Omega = 0.1$ rps. The probe has a radius = 20 mm and mass 40 g (red).

To investigate the difference between the behavior of rising and sinking probes, we plot the viscosity ($\eta(z)$) as a function of probe depth for $H = 50$ and 60 mm (Fig. 5). For sinking probes which are light enough to float, we find that the viscosity is constant and independent of the probe depth. In contrast, the viscosities obtained for rising probes are not constant: the system is less viscous when the probe is deeper. However, the viscosity increases as the probe rises, achieving the viscosity experienced by the sinking probe when the probe reaches the equilibrium depth.

Because the probe is never completely submerged in the grains, the processes of sinking and rising are asymmetric: a sinking probe compresses the grains below it, while a rising probe moves upward and allows the grains beneath to dilate. Because loosely packed grains rearrange more easily than densely packed grains, the motion of sinking probe is impaired as the beads underneath the probe compact, while the motion of a rising probe is effected more easily as the beads under the probe dilate. In the remainder of this paper we will examine the motion of sinking probes.

B. How the viscosity depends on Ω, H, z, M, and R

We have seen that the drag forces on moving probes scale linearly with the probe speed, allowing us to define an effective viscosity for the granular liquid. In this section we describe the results of a series of experiments where we use the probe trajectory $z(t)$ to determine the effective viscosity $\eta(z)$ for a wide range of the control parameters M, R, H, and Ω. Unlike ordinary Newtonian fluids, where the viscosity is independent of the diameter and the mass of the sinking object, we find that the effective viscosity of our granular system depends on M and R.

The relationships between the viscosity and the control parameters are summarized here and and discussed in detail in the following sections. First, we find evidence that the humidity and surface properties of the beads contribute to run-to-run variation in the probe trajectories but do not have a significant effect on the viscosity. Second, we find that the viscosity scales as Ω^{-1} over several orders of magnitude (Sec. IV B1). We also find that the viscosity of the granular liquid depends on the filling height H: increasing the amount of beads in the container strongly increases the viscosity of the beads. In addition, we observe that the viscosity varies weakly with

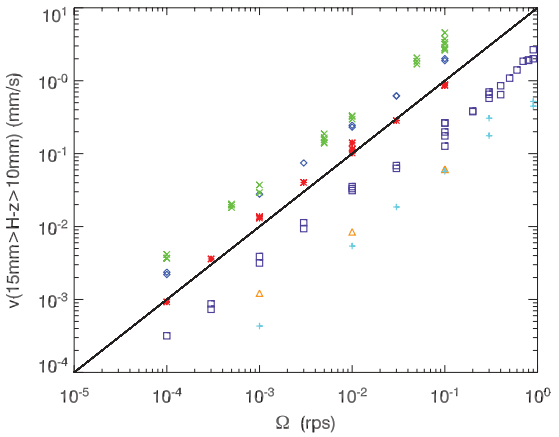

FIG. 6. (Color online) Probe velocity v measured between 10 and 15 mm below the surface, as a function of disk rotation rate. Red stars: $H = 60$ mm, $M = 77$ g, $R = 9$ mm; blue diamonds: $H = 50$ mm, $M = 46$ g, $R = 9$ mm; purple squares: $H = 60$ mm, $M = 48$ g, $R = 9$ mm; green crosses: $H = 60$ mm, $M = 86$ g, $R = 9$ mm; orange triangles: $H = 60$ mm, $M = 46$ g, $R = 9$ mm with a probe immersed at a radius of 15 mm away from the center; light blue plus signs: $H = 70$, $M = 145$ g $R = 15$ mm. The black line denotes a linear relation.

the vertical position of the probe z, and that this variation is dependent on the filling height (Sec. IV B2). In Sec. IV B3 we investigate how the viscosity depends on the mass (M) and radius (R) of the probe. While it is not possible to vary the probe mass and radius over several decades, our observations are consistent with a scaling law: $\eta \sim R^4 M^{-2}$.

1. *Viscosity scales inversely with the disk rotation rate*

The observation that there is no probe motion when the disk is stationary invites questions about how the viscosity changes as the disk rotation rate is decreased. Is there a transition from liquid-like behavior to solid-like behavior at a small, but finite, disk rotation rate?

We have investigated this question by measuring the probe velocity for probes of different mass and diameter at different disk rotation speeds. We focus here on the speed of these probes in a small z interval ($15 > H - z > 10$ mm). As Fig. 6 shows, the probe velocity is proportional to Ω over a wide range of driving rates, irrespective of filling height H, probe dimension r, and mass m; even when the probe is moved off-center this linear scaling persists.

Because the probe velocity is proportional to the disk rotation speed [Eq. (5)] we conclude that the viscosity is inversely proportional to Ω for a broad range of disk rotation rates: $1/\Omega$ selects the time scale for the probe motion. Another way to think of this is that the displacement of a sinking probe depends only on the total strain applied, not on the strain rate; a probe will sink the same distance in one revolution of the disk, no matter how quickly the disk is moving.

2. *How the viscosity depends on H and z*

One striking observation is that the adding grains to the container significantly increases the viscosity at a given

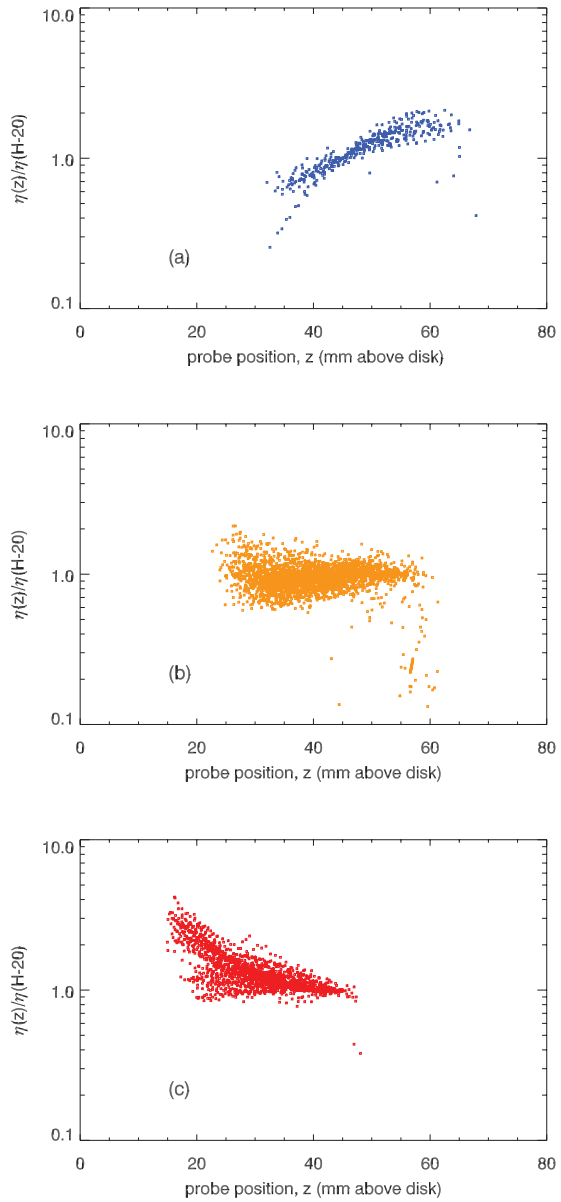

FIG. 7. (Color online) Rescaled viscosity for different filling heights. (a) $[\eta(z)/\eta(40)]$, $H = 70$ mm (top). (b) $[\eta(z)/\eta(55)]$, $H = 60$ mm (middle). (c) $[\eta(z)/\eta(45)]$, $H = 50$ mm (bottom).

distance from the disk; increasing H by one centimeter increases the viscosity by an order of magnitude.

Meanwhile, the viscosity varies weakly with the depth: in Fig. 7 we plot $\eta(z)/\eta(H-5)$ for filling heights of $H = 50$, 60, and 70 mm. For $H = 50$ mm the viscosity is larger when the probe is closer to the rotating disk than at the surface, while for $H = 70$ mm the viscosity is larger when the probe is closer to the surface than near the rotating disk. Meanwhile, the viscosity is fairly constant for all depths reached by the probe at a filling height of $H = 60$ mm.

Note that the heaviest probes experience the greatest viscosity increase as they sink in a system with $H = 50$ mm. This might indicate that the heavy probes are compressing the grains in the region directly above the spinning disk, making it more difficult for the grains beneath the probe to evacuate and allow the probe to sink. Conversely, at $H = 70$ mm, the viscosity for light and heavy probes is slightly greater at the surface than deeper in the material. Note that at $H = 70$ mm, a probe with a length of 4 cm cannot probe deeper than $z = 30$ mm, well above the dome of beads corotating with the disk. At $H = 70$ mm a probe nears the shear band as it sinks: if the shear band generates the fluctuations which cause the grains to fluidize, then a probe might be expected to observe a lower viscosity closer to the shear band than at the surface. Testing these hypotheses requires information about how individual particles move; a measurement might be accomplished with a 3D scanner.

Because the way that the viscosity changes as a function of depth for $H = 60$ and 70 mm is the same for all probe masses and radii, we can express the viscosity as the product of separable functions which depend on the experimental parameters: $\eta = (1/\Omega)F(H,z)G(M,R)$. For $H = 60$ mm F is essentially a constant for all z, while for 70 mm it varies only over a factor of two. Because the viscosity increases more for heavy probes than for light probes as they sink from the surface at $H = 50$ mm we cannot express the viscosity as a product of separable functions. Since the probe is well within the shear band when it is nearly submerged at $H = 50$ mm, we will focus our subsequent analysis on the behavior of probes at larger filling heights.

3. How the viscosity depends on M and R

In this section we explore how the effective viscosity varies with the mass and radius of the probe for $H = 60$ and 70 mm. We find that the viscosity decreases strongly with M and increases strongly with R. During experiments in which examine how the viscosity is affected by M and R we select disk rotation rates, Ω, so that the probes do not not require onerous amounts of time to sink. Because the viscosity is known to scale as $1/\Omega$ (Sec. IV B1), we can compare runs at different rotation speeds by examining the product $\Omega\eta$.

Examples of the viscosity $\eta(z)$ for a range of masses are given in Fig. 8(a) ($H = 60$ mm) and Fig. 8(d) ($H = 50$ mm). Since η does not vary strongly with z for $H = 60$ mm, we can plot the rescaled viscosities $\Omega\eta(z = H - 20\,\text{mm})$ as a function of M for different probe radii [Fig. 8(b) and 8(e)]. Although there clearly is substantial scatter in the data, and the range of M is limited, the relationship between the viscosity and the probe mass is consistent with a simple scaling law: $\Omega\eta \sim M^{-2}$.

It is difficult to measure how the viscosity depends on the probe radius because the probes must be smaller than the container and large enough to float. Measurements for probes with $9 < R < 30$ mm suggest that the relationship between the viscosity and probe radius is consistent with a power law where the viscosity is proportional to R^4 [Fig. 8(b) and 8(e)].

Since the viscosity is roughly proportional to M^{-2} and R^4, the viscosity experienced by sinking probe appears to scale inversely with the square of the pressure exerted by the probe: for $H = 60$ mm, $\eta \approx 1.9 \times 10^3 \pm 7 \times 10^2$ Pa g^2/mm^4 $\Omega^{-1}M^{-2}R^4$, while for $H = 70$ mm, $\eta = 1.2 \times 10^4 \pm 3 \times 10^3$ Pa g^2/mm^4 $\Omega^{-1}M^{-2}R^4$ [Fig. 8(c) and 8(f)].

Using the motion of sinking probes, we have measured the viscosity of a granular system excited by shear. We find that the viscosity increases as the filling height of the grains in the container is increased. The viscosity of a sinking probe is

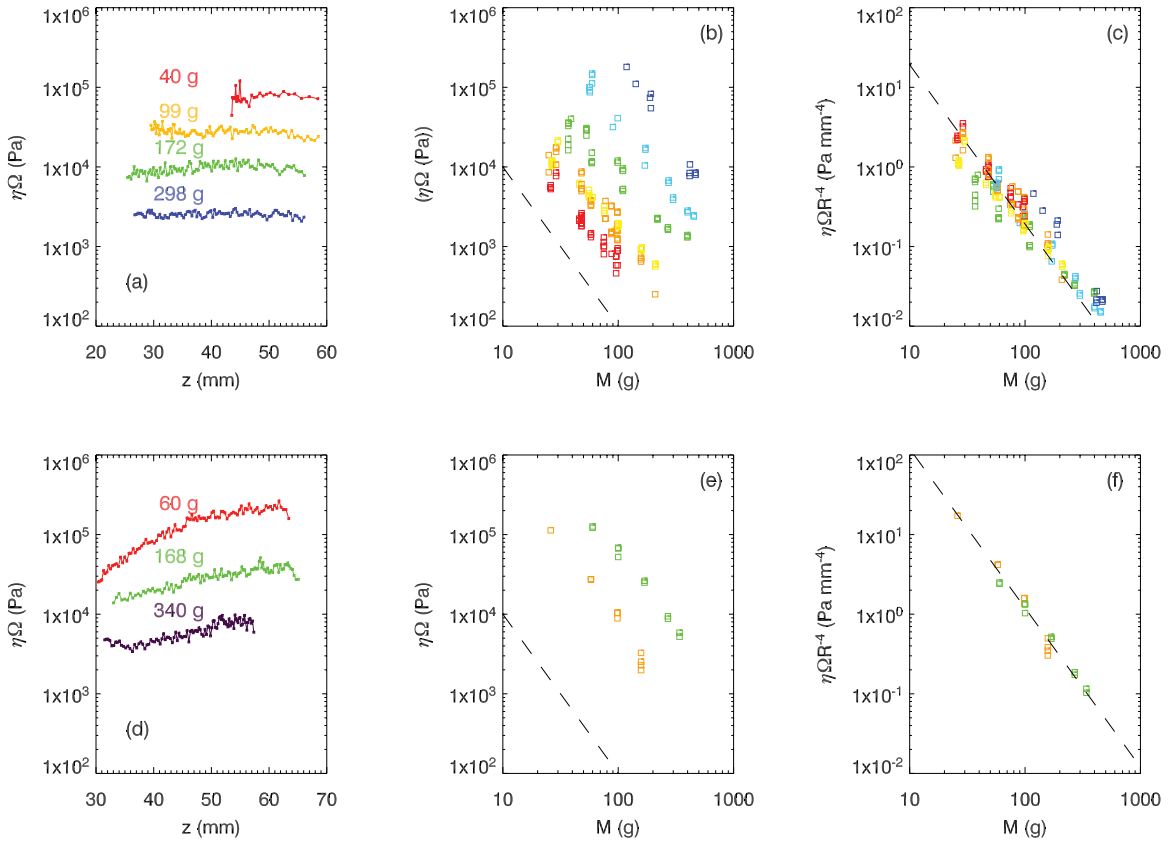

FIG. 8. (Color online) Scaling of the viscosity with M and R. (a–c) $H = 60$ mm. (a) $\eta(z)$ for a range of probe masses for $R = 20$ mm. (b) Rescaled viscosity $\Omega\eta(z = H - 20)$ as a function of mass for several probe radii (from bottom to top: red: $R = 7$ mm; orange: $R = 9$ mm; yellow: $R = 10$ mm; green: $R = 15$ mm; cyan: $R = 20$ mm; blue: $R = 25$ mm). In panels (b), (c), (e), and (f) the dashed line is a guide to the eye and has slope -2. (c) The rescaled viscosity $\Omega\eta(z = H - 20)R^{-4}$ scales as $(1.9 \times 10^3 \pm 7 \times 10^2)$ Pa g^2/mm^4 M^2. (d–f) $H = 70$ mm. (d) $\eta(z)$ for a range of probe masses for $R = 25$ mm. (e) Rescaled viscosity $\Omega\eta(z = H - 20)$ as a function of mass for two values of R [highest dataset (green) $R = 15$ mm; lowest dataset (orange) $R = 9$ mm]. (f) The rescaled viscosity $\Omega\eta(z = H - 20$ mm$)R^{-4}$ scales in as $1.2 \times 10^4 \pm 3 \times 10^3$ Pa g^2/mm^4 M^2.

constant for $H = 60$ mm and decreases slightly as the probe sinks in a system with $H = 70$ mm. The viscosity experienced by a sinking object can be related to the mass and radius of the object and the rotation rate of the disk with a simple power law: $\eta \propto \Omega^{-1} R^4 M^{-2}$.

C. Does the local flow rate set the viscosity?

Even though the flow at the surface is very slow, it is not zero [6,11,12]. It is therefore natural to ask whether the probe motion is determined by the local flow near the probe: either the local strain rate or the flow rate past the probe. We can probe this question by comparing the r and z dependencies of the local flow and strain rates to the spatial variation of the effective viscosity.

We first focus on the case of probes immersed in the center ($R = 0$) of the system, thus focusing on the variation with z and H. For dome-like shear bands, the strain in the region above the center of the disk is torsional [12], and so the strain rate varies as $(\partial_z \omega|_{R=0})$. In Fig. 9 we compare the viscosities and local strain rates.

Local strain rates—We have measured the precession rate $\omega_p(z) := \omega(z)|_{R=0}/\Omega$ by inserting a vane in the center of the grain flow and observing the rotation of the probe with an Anton Paar DSR 100 rheometer. The vanes consist of four rectangular blades of height 10 mm and radius 5 mm mounted on a smooth rod. By removing the blades from this rod we have established that the torques exerted on the rod are two orders of magnitude smaller than those exerted on the vane: in very good approximation the measured rotation of the vane follows the flow near the vane and is insensitive to the rest of the rod which is submerged in the grains. We also find that varying the dimensions of the vane produces no systematic changes in the measured precession rates.

The resulting vane precession rates, $\omega_p(z)$, are shown in Fig. 9(a) for $H = 50$,60, and 70 mm and are in reasonable qualitative agreement with earlier magnetic resonance imaging measurements and simulations [12]. Because our measurements of the precession rates are made over a larger range, we can establish that $\omega_p(z)$ approaches the surface precession rate, $\omega_p(z = H)$, more quickly than an exponential but more slowly than a Gaussian, and our results are fitted well by an expression of the form

$$\omega_p(z) - \omega_p(z = H) = \omega_p(z = 0) \exp[-(z/\xi)^{1.5}], \qquad (7)$$

where $\omega_p(z = 0)$ captures slip near the bottom disk, and the characteristic length scale ξ is of order 10 mm.

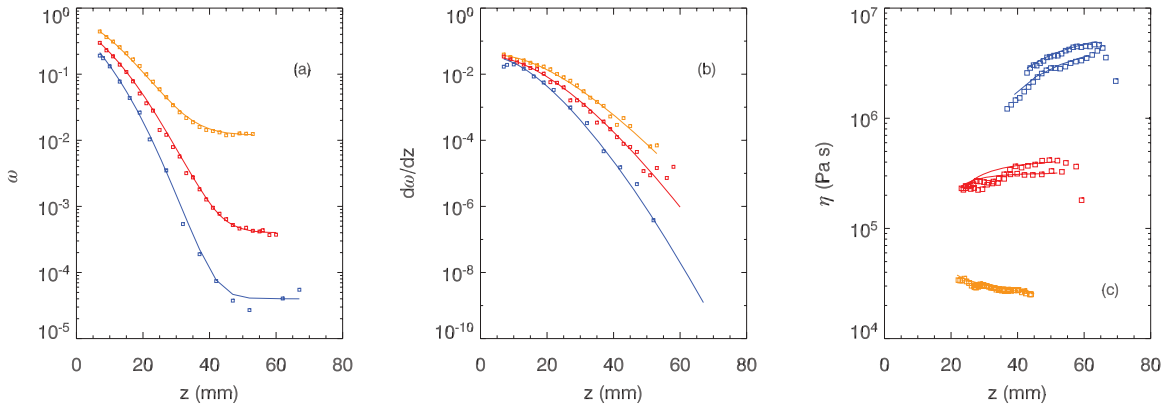

FIG. 9. (Color online) (a) ω_p as a function of the height above the spinning disk for $H=50$ mm (top curve, orange), $H=60$ mm (middle curve, red), and $H=70$ mm (bottom curve, blue). Curves are of the form $\omega_p(z)-\omega_p(z=H)\sim\exp(-(z/\xi)^{1.5})$, with $\xi=9.5,11.5$, and 13 mm, respectively. Note that the plateaus of $\omega_p(z)$ for $z\to H$ correspond to the precession rates measured, by video imaging, at the free surface [21]. (b) The corresponding variation of the strain rate $\partial_z\omega_p$ with z for $H=50,60$, and 70 mm (top to bottom curve). (c) Viscosity as a function of probe position for a probe with $M=59$ g, $D=30$ mm, and $H=50,60$, and 70 mm (lower orange curve, middle red curve, and upper blue curve, respectively).

In Fig. 9(b) we show the corresponding values of the strain rates, $(\partial_z\omega|_{R=0})$. Data obtained by numerically differentiating the measured ω are shown as individual data points, and the curves follow from directly differentiating the fit Eq. (7). The two estimates for the strain rate are in excellent agreement and show that the local strain rate varies over several decades as a function of z.

In Fig. 9(c) we show three examples of the local viscosities for a single probe ($M=59$ g, $R=15$ mm), and for filling heights of 50, 60, and 70 mm, respectively. Clearly the local strain rate and $\eta(z)$ correlate very poorly: the local strain rate changes over four decades for $H=70$ mm, while $\eta(z)$ changes over less than half a decade. This suggests that the liquid-like behavior of a granular system fluidized by shear is not caused by local flow near a sinking object.

1. *Moving the probe from the center of the setup*

We have also explored the effect of moving the probe away from the center of the setup. Away from the center, the material continues to behave as a viscous fluid and demonstrates no yield stress; however, the effective viscosity increases away from the center of the cell. This is illustrated in Fig. 6 where we compare the velocity of a sinking probe of radius 9 mm in the center of the system (purple squares) to the velocity of an identical sinking probe displaced 15 mm from the center (orange triangles); the sinking speed of the latter probe decreases by about a factor of four.

This observation suggests that the local flow past the probe is not the cause of the fluid-like behavior, since the local flow speed *increases* with the radial distance r, but the viscosity observed by a sinking object *decreases* with r.

In conclusion we find that neither the local strain rate nor the local rate of flow past the probe are good predictors for the observed effective viscosity. This strongly suggests a nonlocal source of fluidization, in which the strain rate in one location (in the shear band) governs the effective viscosity of the granular materials far from the shear band.

V. FLUCTUATIONS

In the previous section we showed that the local flow and strain rates do not correlate well with the local viscosity. We therefore propose that *fluctuations* are responsible for causing the liquid-like behavior of the grains. In the following section we probe grain motion by observing fluctuations in the trajectories $z(t)$ of floating probes. Except for probes that are precisely at their equilibrium depth, there is a need to separate the slow motion of the probe from the random fluctuations. To do so, we first subtract off the decay envelope which stems from the viscous sinking process [Fig. 10(a)]. In addition, we filter out a small characteristic oscillation due to a tiny misalignment of the spinning disk. A resulting typical time trace for Δz is shown in Fig. 10(a).

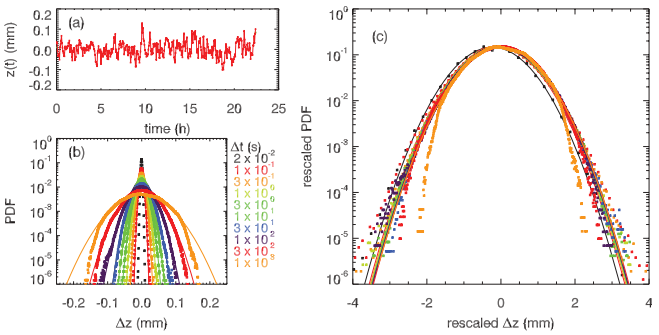

FIG. 10. (Color online) Fluctuations. (a) The fluctuations are given by the difference between probe position and fit. (b) Distribution of displacements, $\Delta z(\Delta t)$, for a range of time intervals as indicated in the legend: the larger the time interval, the wider the PDF. The data are for a probe ($R=25$ mm, $M=30$ g) floating in grains with height $H=55$ mm and driven at $\Omega=0.1$ rps. The data set is 11.6 h in duration and sampled at 50 Hz. The bin size of the PDFs is 6.7×10^{-4} mm. (c) The PDFs are rescaled by their width and height, and the resulting distributions are all Gaussian with the exception of the data for $\Delta t\geqslant300$ s where the distributions are slightly narrower.

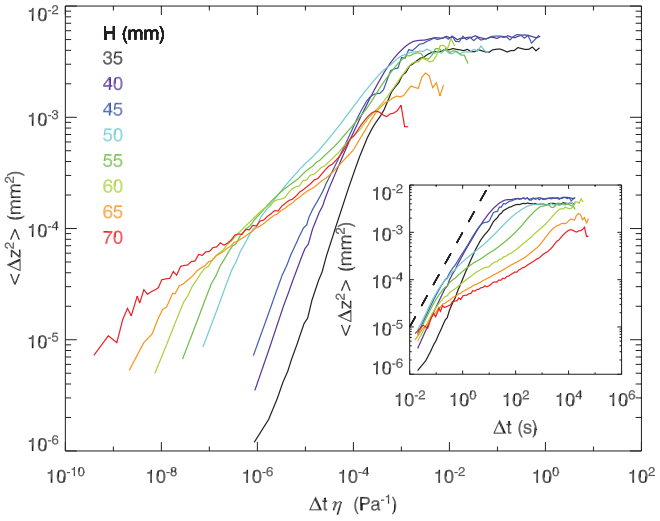

FIG. 11. (Color online) Time evolution of the mean square displacements $\langle \Delta z^2 \rangle$ for $M = 30$ g, $R = 25$ mm, and $\Omega = 0.1$ rps for filling heights ranging from $H = 35$ to 70 mm as indicated. The main panel shows that the crossover time to the plateau rescales with the effective viscosity. For increasing H, the curves at early times shift to the left. Inset: Raw data; for increasing H the curves shift to the right. The dashed line indicates a diffusive mean square displacement curve.

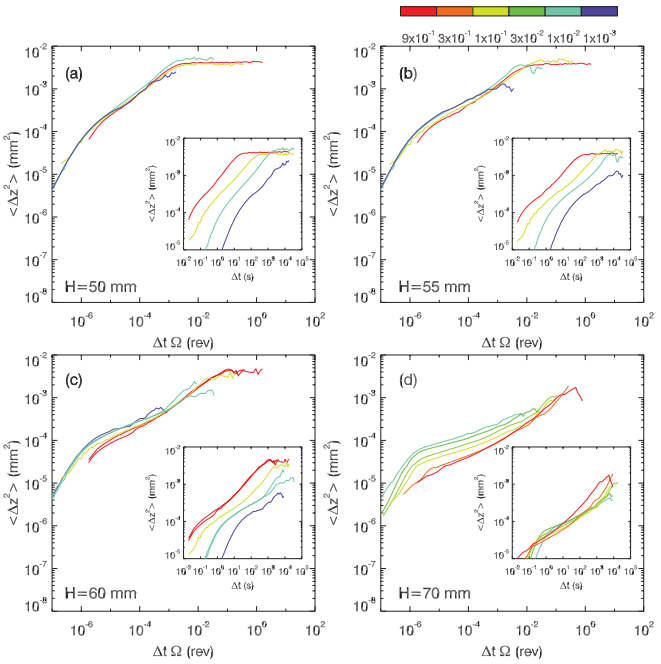

FIG. 12. (Color online) Mean square displacement for $\Omega = 0.9, 0.1, 0.01$, and 0.001 rps. (a) $H = 50$ mm, $R = 25$ mm, $M = 56$ g (in the inset, curves shift to the right with increasing Ω). (b) $H = 55$ mm, $R = 25$ mm, $M = 56$ g (in the inset, curves shift to the right with increasing Ω). (c) $H = 60$ mm, $R = 25$ mm, $M = 36$ g (in the inset, curves shift to the right with increasing Ω). (d) $H = 70$ mm, $R = 25$ mm, $M = 36$ g (in the inset, curves appear to shift downward with increasing Ω).

We have explored the probability distribution functions of the random displacements Δz in detail, and for all time intervals that we can probe, and for all experimental parameters, we have found that these distributions are essentially Gaussian, with the exception of very large time intervals, where the tails of the distributions are slightly underpopulated [Figs. 10(b) and 10(c)]. In the remainder we therefore focus on the time evolution of the mean square displacements $\langle \Delta z(\Delta t)^2 \rangle$.

Effect of the filling height—The mean square displacement curves for systems with different filling heights are compared in Fig. 11. For low filling heights ($H = 35,40$ mm) the evolution of the mean squared displacements is nearly diffusive at short times, while subdiffusive behavior emerges for larger filling heights. The presence of diffusive behavior at low filling heights appears to be related to the fact the system with $H < 45$ mm has a significant amount of flow at the surface; for low filling heights the shear bands extend to the surface.

On long time scales the mean squared displacements saturate. This plateau can be expected because the probe is "walking" in a potential well given by the gravitational force and the buoyant force on the probe. The mean squared displacements in this plateau are of order 10^{-2} mm^2, consistent with the size of the square of the largest fluctuations in $z(t)$ in Fig. 10.

We have now shown that both the effective viscosity as well as the mean square displacements strongly vary with the filling height H. In Fig. 11 the time axis of the MSD curves are rescaled by the viscosities determined from the corresponding sinking probe trajectories, and we find that the crossover regions overlap. This suggests that the characteristic time scales of the viscosity and fluctuations are deeply related.

Effect of the driving rate—The effective viscosity scales trivially with the driving rate Ω: what about the fluctuations? When we rescaled the time axis for the MSD curves by the disk rotation speed (Fig. 12) the curves at lower filling heights ($H <$ =60) overlap at all time scales, although some deviations from this scaling can be seen for larger filling heights and early times; even when the rescaling is not perfect, the crossover to the plateau regime is well captured for all filling heights. This suggests that it is the time scale at which the plateau appears which is important in setting the viscosity.

Effect of the probe mass—Predictions about the effect of the probe mass and diameter can be made by considering the Ornstein-Uhlenbeck theorem, which models the behavior of a random walker in a potential well [25]. Even though the probe motion here is not Brownian, the mean square displacement curves exhibit a plateau, and so we may ask whether the characteristics of this plateau are consistent with the scalings predicted by the Ornstein-Uhlenbeck theorem.

The potential well occupied by the floating probe has the form $U = -1/2\rho g R^2 \pi (z - z_{\rm eq})^2$, where $z_{\rm eq}$ is the equilibrium depth predicted by Archimedes' law. The width of the potential well is therefore determined entirely by the probe radius: varying the mass of the probe changes $z_{\rm eq}$ and simply shifts the potential up and down. Since the effective elastic constant, $k = \pi \rho g R^2$, is independent of the probe mass, the saturated value of the MSD in the plateau should also be independent of the probe mass.

At $H = 60$ mm (Fig. 13) the starting points of the plateaus are not distinguishable from each other, and at $H = 50$ there is no systematic dependence of the turn-off position on the probe mass. Since the mean square displacement curves are

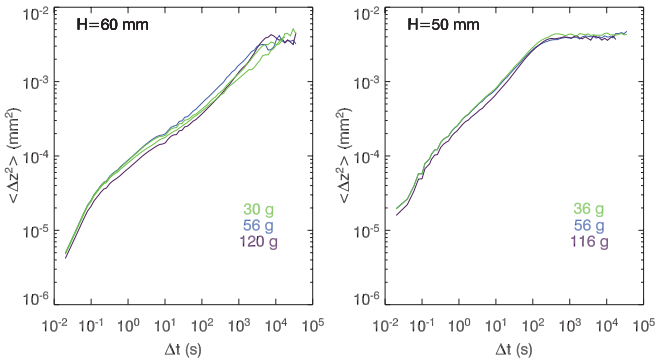

FIG. 13. (Color online) Left panel: $\langle(\Delta z)^2\rangle$ for $H = 60$ mm, $R = 25$ mm, and $M = 30$ g, $M = 56$ g, and $M = 120$ g overlap. Right panel: $\langle(\Delta z)^2\rangle$ for $H = 50$ mm, $R = 25$ mm, and $M = 36$ g, $M = 56$ g, and $M = 116$ g overlap.

not significantly changed by tuning the mass of the probe, the fluctuations experienced by the probe do not appear to be affected by the mass of the probe.

Probe depth—Examining the MSD curves and PDFs for a single probe that is either sinking or rising (Fig. 14) allows us to probe how the fluctuations are affected by both the probe motion and the probe position. Even though a small shift in the fluctuation strength [similar in magnitude to the vertical variation in the local viscosity; see Fig. 9(c)] can be seen for $H = 70$ mm, the overall effect of the probe position on the fluctuations is weak. This weak dependence of the

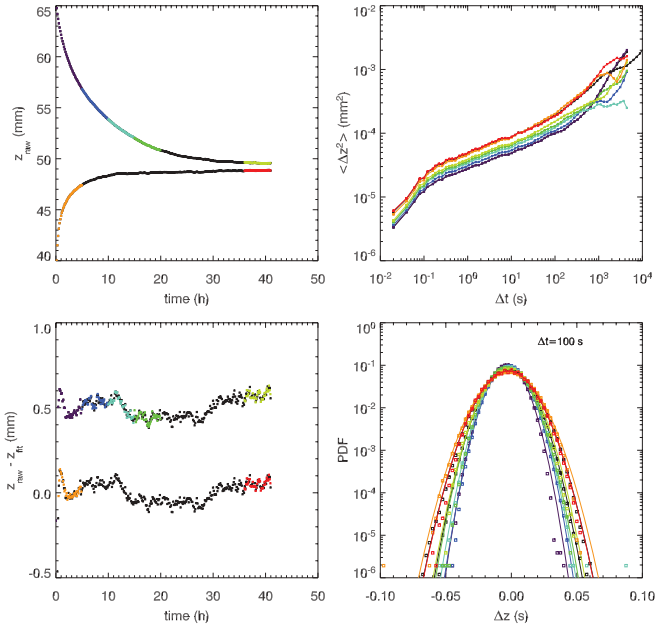

FIG. 14. (Color online) Top left: Raw probe position $[z_{\rm raw}(t)]$ for a sinking probe and rising probe experiment. $H = 70$ mm, $M = 85$ g, $R = 25$ mm, $\Omega = 0.1$ rps. Lower left: Probe position after a fit to the sinking (or rising) motion, $z_{\rm fit}(t)$, is subtracted: $z_{\rm raw}(t) - z_{\rm fit}(t)$. Top right: The mean square displacement curves for different probe depths; the color (shade of gray) corresponds to the segment of the raw data in the upper left panel, and curves lie lower for increasing values of z. Lower right: PDFs for each segment of the data set ($\Delta t = 100$ s); PDFs are narrower for increasing values of z.

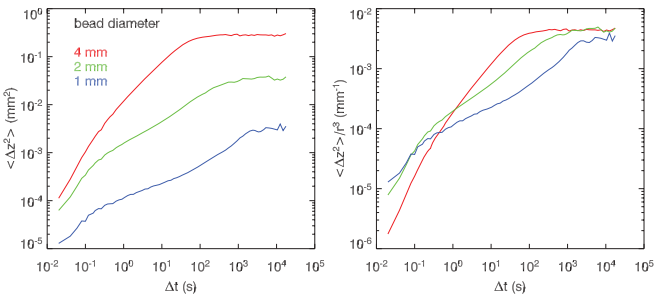

FIG. 15. (Color online) Left panel: $\langle\Delta z^2\rangle$ for beads of different diameters d_b (Top: $d_b = 4$ mm, middle: $d_b = 2$ mm, bottom: $d_b = 1$ mm). $H = 60$ mm, $R = 25$ mm, $M = 56$ g, $\Omega = 0.1$ rps. Right panel: The plateau position is proportional to the volume of a single bead. The observed equilibrium depths for our probe where $z \approx 46$, $z \approx 45$, and $z = \approx 49$ mm for the $d_b = 1$, 2, and 4 mm beads. We estimate $z_{\rm eq}$ at 46 ± 1 mm, and taking error bars of order $\pm d_b$, we conclude that all data are consistent with Archimedes' law.

fluctuations on z is further evidence that the local flow does *not* set the fluctuations. It also supports the idea that the fluctuations set the viscosity, which have a similar weak z dependence. In addition, we find that for $H = 60$ mm (data not shown) the magnitude of the fluctuations is similar for all probe depths. This observation is concomitant with the z-independent viscosity observed for $H = 60$ mm [Fig. 9(c)].

Role of bead size—As Fig. 15 illustrates, the particle size sets the value of the MSD in the plateau. For the limited range of bead diameters that we can probe, we find that the magnitude of the MSD fluctuations scales with the particle volume, or equivalently, with the particle mass. This is similar to what would be expected from the Ornstein-Uhlenbeck theorem, if we assume that the effective temperature is proportional to the mass of a single particle.

VI. CONCLUSION

In this paper we have characterized both the overall motion and fluctuations of probes immersed in a granular system excited by shear: a system which has many of the properties of a liquid.

By comparing the equilibrium depth of a low-density object rising in the grains to the equilibrium depth of that same object sinking in the grains we have demonstrated that our granular liquid does not exhibit a yield stress. We have also observed that the equilibrium depth can be predicted by Archimedes' law.

In addition to examining the equilibrium behavior of the floating probe, we have found that a moving probe experiences viscous drag, in the sense that probe speed and drag forces are proportional. We note that in recent experiments, Reddy *et al.* [26] have probed drag forces in granular Couette systems. These experiments do not find a linear dependence between drag force and probe motion; we have no explanation for this difference to our system.

We have determined the viscosity of our granular liquid by measuring the vertical position of a sinking object as a function of time. We find that the viscosity of the liquid is inversely proportional to the disk rotation rate. We have also

observed that increasing the filling height of the beads in the container increases the viscosity.

We have observed two unliquid-like behaviours in our granular system. First, the viscosity of a real liquid is independent of the diameter and the mass of the sinking object, but here we find that the viscosity of our granular system varies with the mass and diameter of the probe. Our observations suggest that the way the viscosity depends on the probe mass and radius can be described by a power law: $\eta \propto r^4 m^{-2}$. The viscosity therefore appears to be proportional to the pressure exerted by the probe. Second, the viscosity experienced by a rising probe is slightly smaller than the viscosity experienced by a sinking probe. We note that it may be the case that the grains have more difficulty rearranging when they are compressed by a sinking probe than when they dilate under a rising probe.

By comparing the local variations in local flow rate and viscosity we have demonstrated that the viscosity is not simply set by the local flow rate, which suggests a nonlocal rheology in the sense that there cannot be a local relation between stress and strain rate that governs the rheology. Rather, we believe that fluctuations mediate interactions between spatially separated regions.

We have probed these fluctuations by probing the fluctuations in probes that are floating or sinking into the medium. In all cases these fluctuations were found to Gaussian, so we have focused on the mean squared displacements as function of time interval. We extract several features from these. First, after a short time interval of nearly diffusive behavior, the motion of the probe is subdiffusive and becomes more subdiffusive as the filling height increases. Interestingly, the presence of Gaussian PDFs *and* subdiffusive behavior is characteristic of neither a glass [27–33] nor a simple liquid! Second, the value of mean square displacements saturates at long time scales. The appearance of this plateau is concomitant with the behavior of a simple random walker in a potential well described by the Ornstein-Uhlenbeck theorem. We find that the plateau values of the mean square displacement curves scale with the probe radius but are independent of the probe mass, suggesting that the potential well traversed by the probe is given by the buoyant and gravitational forces. Third, we have found that the time scales at which the plateaus begin are proportional to the viscosity of the system. This behavior is apparent both in the case where the viscosity is varied by changing the disk rotation speed and in the case where the viscosity is varied by changing the filling height. That time scale of the viscosity and the time scale of the fluctuations are the same suggests that fluctuations determine the viscosity of the system.

We have also examined how the fluctuations change with probe position: we have studied both the equilibrium behavior of probes with different masses and the motion of sinking probes away from the equilibrium position. Our results suggest that the magnitude of the fluctuations does not vary significantly throughout the system and does not vary much when the probe is away from the equilibrium position.

The picture that is emerging is that slow granular flows are governed by principles very different from the simple Mohr-Coulomb picture. The essence is that the local strain rate is governed not only by the local stress, but also by the local amount of agitations. These agitations are generated in flowing regions in the system and spread far through the granular medium. These two simple ingredients capture most of our findings and provide key ingredients for the development of better models of slow granular flows [15–17].

ACKNOWLEDGMENTS

The authors wish to thank Elie Wandersman for experimental input, Brian Tighe, Wim van Saarloos, and Mike Cates for discussions, and Jeroen Mesman for his technical assistance. This work is part of the research program of the Foundation for Fundamental Research on Matter (FOM), which is part of the Netherlands Organisation for Scientific Research (NWO).

APPENDIX: FITTING THE PROBE POSITION AS A FUNCTION OF TIME

Although the solution to Eq. (3) is an exponential, plotting the velocity as a function of time suggests (Fig. 16) that the probe initially sinks more quickly than expected. This can be modeled by introducing a second exponential into the fit. This fit is useful for extracting the equilibrium depth, z_{eq}:

$$z(t) = a_1 e^{-k_1 t} + a_2 e^{-k_2 t} + z_{\mathrm{eq}}. \tag{A1}$$

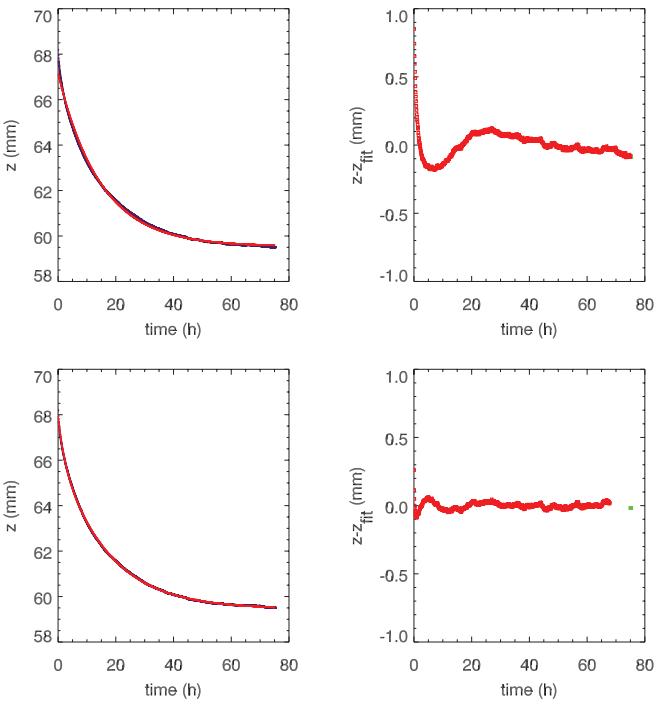

FIG. 16. (Color online) The fit to two exponentials (lower two panels) captures the early time behavior better than the fit to one exponential (upper panels). The raw data and the fits are displayed in the left-hand panels, and the residuals are plotted in the right-hand panels ($H = 65$ mm, $\Omega = 0.1$, $M = 36$ g, $R = 25$ mm).

[1] H. M. Jaeger, S. R. Nagel, and R. P. Behringer, Rev. Mod. Phys. **68**, 1259 (1996).
[2] I. Goldhirsch, Annu. Rev. Fluid Mech. **35**, 267 (2003).
[3] GDR MiDi, Eur. Phys. J. E **1**, 341 (2004).
[4] P. Jop, Y. Forterre, and O. Pouliquen, Nature (London) **441**, 727 (2006).
[5] R. M. Nedderman, *Statics and Kinematics of Granular Materials* (Cambridge University Press, Cambridge, 1992).
[6] T. Unger, J. Török, J. Kertész, and D. E. Wolf, Phys. Rev. Lett. **92**, 214301 (2004).
[7] R. R. Hartley and R. P. Behringer, Nature (London) **421**, 928 (2003).
[8] D. M. Mueth, G. F. Debregeas, G. S. Karczmar, P. J. Eng, S. R. Nagel, and H. M. Jaeger, Nature (London) **406**, 385 (2000).
[9] T. S. Komatsu, S. Inagaki, N. Nakagawa, and S. Nasuno, Phys. Rev. Lett. **86**, 1757 (2001).
[10] L. Bocquet, W. Losert, D. Schalk, T. C. Lubensky, and J. P. Gollub, Phys. Rev. E **65**, 011307 (2001).
[11] D. Fenistein and M. van Hecke, Nature (London) **425**, 256 (2003).
[12] X. Cheng, J. B. Lechman, A. Fernandez-Barbero, G. S. Grest, H. M. Jaeger, G. S. Karczmar, M. E. Mobius, and S. R. Nagel, Phys. Rev. Lett. **96**, 038001 (2006).
[13] J. Crassous, J.-F. Metayer, P. Richard, and C. Laroche, J. Stat. Mech. (2008) P03009.
[14] J. Goyon, A. Colin, G. Ovarlez, A. Ajdari, and L. Bocquet, Nature (London) **454**, 84 (2008).
[15] L. Bocquet, A. Colin, and A. Ajdari, Phys. Rev. Lett. **103**, 036001 (2009).
[16] M. Depken, W. van Saarloos, and M. van Hecke, Phys. Rev. E **73**, 031302 (2006); M. Depken, J. B. Lechman, M. van Hecke, W. van Saarloos, and G. S. Grest, Europhys. Lett. **78**, 58001 (2007).
[17] R. Gutfraind and O. Pouliquen, Mech. Mater. **24**, 273 (1996).
[18] J. Török, T. Unger, J. Kertész, and D. E. Wolf, Phys. Rev. E **75**, 011305 (2007).
[19] A. Ries, D. E. Wolf, and T. Unger, Phys. Rev. E **76**, 051301 (2007).
[20] D. Fenistein, J.-W. van de Meent, and M. van Hecke, Phys. Rev. Lett. **92**, 094301 (2004).
[21] D. Fenistein, J.-W. van de Meent, and M. van Hecke, Phys. Rev. Lett. **96**, 118001 (2006).
[22] J. A. Dijksman and M. van Hecke, Granular Flows in Split-Bottom Geometries Soft Matter **6**, 2901 (2010).
[23] W. N. Man, A. Donev, F. H. Stillinger, M. T. Sullivan, W. B. Russel, D. Heeger, S. Inati, S. Torquato, and P. M. Chaikin, Phys. Rev. Lett. **94**, 198001 (2005).
[24] D. A. Huerta, V. Sosa, M. C. Vargas, and J. C. Ruiz-Suárez, Phys. Rev. E **72**, 031307 (2005).
[25] G. E. Uhlenbeck and L. S. Ornstein, Phys. Rev. **36**, 823 (1930).
[26] K. A. Reddy, Y. Forterre, and O. Pouliquen, Phys. Rev. Lett. **106**, 108301 (2011)
[27] H. Katsuragi and D. J. Durian, Nature Phys. **3**, 420 (2007).
[28] R. Candelier and O. Dauchot, Phys. Rev. Lett **103**, 128001 (2009).
[29] J. F. Geng and R. P. Behringer, Phys. Rev. E **71**, 011302 (2005).
[30] J. B. Knight, C. G. Fandrich, C. N. Lau, H. M. Jaeger, and S. R. Nagel, Phys. Rev. E **51**, 3957 (1995).
[31] P. Umbanhowar and M. van Hecke, Phys. Rev. E (R) **72**, 030301 (2005).
[32] O. Dauchot, G. Marty, and G. Biroli, Phys. Rev. Lett. **95**, 265701 (2005).
[33] A. S. Keys, A. R. Abate, S. C. Glotzer, and D. J. Durian, Nature Phys. **3**, 260 (2007).